Lab on a Chip

PAPER

View Article Online
View Journal | View Issue



Cite this: *Lab Chip*, 2024, **24**, 854

# Modelling and breaking down the biophysical barriers to drug delivery in pancreatic cancer†

Delanyo Kpeglo, [a] Malcolm Haddrick,[c] Margaret A. Knowles,[b] Stephen D. Evans [a] and Sally A. Peyman *[ab]

The pancreatic ductal adenocarcinoma (PDAC) stroma and its inherent biophysical barriers to drug delivery are central to therapeutic resistance. This makes PDAC the most prevalent pancreatic cancer with poor prognosis. The chemotherapeutic drug gemcitabine is used against various solid tumours, including pancreatic cancer, but with only a modest effect on patient survival. The growing PDAC tumour mass with high densities of cells and extracellular matrix (ECM) proteins, *i.e.*, collagen, results in high interstitial pressure, leading to vasculature collapse and a dense, hypoxic, mechanically stiff stroma with reduced interstitial flow, critical to drug delivery to cells. Despite this, most drug studies are performed on cellular models that neglect these biophysical barriers to drug delivery. Microfluidic technology offers a promising platform to emulate tumour biophysical characteristics with appropriate flow conditions and transport dynamics. We present a microfluidic PDAC culture model, encompassing the disease's biophysical barriers to therapeutics, to evaluate the use of the angiotensin II receptor blocker losartan, which has been found to have matrix-depleting properties, on improving gemcitabine efficacy. PDAC cells were seeded into our 5-channel microfluidic device for a 21-day culture to mimic the rigid, collagenous PDAC stroma with reduced interstitial flow, which is critical to drug delivery to the cancer cells, and for assessment with gemcitabine and losartan treatment. With losartan, our culture matrix was more porous with less collagen, resulting in increased hydraulic conductivity of the culture interstitial space and improved gemcitabine effect. We demonstrate the importance of modelling tumour biophysical barriers to successfully assess new drugs and delivery methods.

Received 28th July 2023,
Accepted 10th January 2024

DOI: 10.1039/d3lc00660c

rsc.li/loc



## Introduction

It is becoming increasingly evident that the tumour microenvironment plays an important role in tumour growth and in drug resistance mechanisms.[1,2] As tumours grow, cancer cells engineer a rigid matrix environment, which promotes cell growth, invasion and metastasis, and therapeutic resistance. One such cancer where the tumour microenvironment is central to its malignancy is pancreatic ductal adenocarcinoma (PDAC).

PDAC is the most common pancreatic cancer, with a median survival of 10–12 months.[2] It is often diagnosed in its advanced stages, where it is characterised by a rigid stroma, constituting 90% of the tumour volume and driving its aggressiveness.[3,4] The rigid stroma stems from the cell–cell interactions between the PDAC cancer cells and stromal cells, primarily pancreatic stellate cells (PSCs), the main fibroblast cells of the pancreas.[5] PSC interactions with the PDAC cancer cells, exacerbated by transforming growth factor-β1 (TGF-β1), results in a growing extracellular matrix (ECM) with abundant fibrous proteins, predominantly collagen.[6,7] The accumulation and cross-linking of these fibrous proteins increases tissue stiffness, decreases matrix porosity, elevates intratumoural pressure, and reduces interstitial flow, which is critical to drug delivery to cancer cells.[4,8]

Surgery, with curative intent, is preceded and followed with neoadjuvant and adjuvant treatments such as the cytotoxic chemotherapeutic gemcitabine, which has modest improvements in patient survival (median survival of 35.0 months).[9,10] For improved treatment interventions, an understanding of the tumour mechanobiology of solid tumours and its role in drug resistance is of vital importance. Hence, the development of appropriate three-dimensional (3D) *in vitro* models that mimic the tumour microenvironment, particularly the rigid fibrotic matrix with its inherent flow and transport

[a] *Molecular and Nanoscale Physics Group, School of Physics and Astronomy, University of Leeds, LS2 9 JT, UK. E-mail: S.Peyman@leeds.ac.uk*
[b] *Leeds Institute of Medical Research at St James's (LIMR), School of Medicine, University of Leeds, LS2 9 JT, UK*
[c] *Medicines Discovery Catapult, Block 35, Mereside Alderley Park, Alderley Edge, SK10 4TG, UK*

† Electronic supplementary information (ESI) available. See DOI: https://doi.org/10.1039/d3lc00660c

properties, is essential to investigate and understand the tumour mechanobiology for effective therapeutic measures.

Two-dimensional (2D) cultures lack the 3D complexity of tissues, and mouse models are genetically and physiologically different to humans, so drug testing results from these models are difficult to translate to the clinic.[11] Reported 3D culture models are often in static well formats, neglecting the important flow and transport characteristics of tissues, such as the presence of interstitial flow that delivers nutrients and drugs deep into tissues and the shear forces associated with these moving fluids. Microfluidic organ-on-chip technology provides the advantage of fluid control within defined geometries, offering an advanced culture platform to accurately build 3D *in vitro* models that mimic the tumour biophysical and hydraulic environment, and to also more accurately assess new drugs and delivery mechanisms.[11,12]

We have previously shown the PDAC tumour stroma, and mechanical stiffness can be recapitulated with the 3D spheroid culture of PDAC cancer cells with PSCs and TGF-β1 supplement for 21 days. By culturing the model for 21 days, we demonstrated an accumulation of collagen in the culture matrix and, therefore, increased matrix stiffness and a hypoxic environment, impacting the delivery of gemcitabine to the cancer cells.[13] However, with the static fluidic nature of the cultures and inability to induce fluid flow, the reduced interstitial flow and transport properties, as seen in the *in vivo* tumour tissue with a dense, rigid collagenous matrix environment, could not be modelled to investigate potential therapeutic strategies, *i.e.*, the use of matrix-depleting drugs, to improve gemcitabine delivery and their effect against the cancer cells. With an in-house fabricated microfluidic device, we grew the PDAC cultures for up to 21 days to achieve mechanical maturity (rigid, collagenous matrix environment) and investigated how this affected interstitial flow, the primary route to deliver drugs to cells. We demonstrated that a 21-day culture, with reduced interstitial flow, has a higher drug resistance to treatment with gemcitabine and evaluated the use of the matrix-depleting drug, losartan, to improve gemcitabine delivery to the cells.

Losartan is an angiotensin II receptor blocker approved to treat high blood pressure. In addition to its anti-hypertensive properties, losartan exhibits anti-fibrotic properties.[14] The matrix-depleting property of losartan is believed to be *via* its inhibition of the TGF-β1 signalling pathway. Losartan acts on angiotensin II type I receptors (AGTR1), suppressing TGF-β1 activators such as thrombospondin-1 (TSP-1). The suppression of TSP-1 levels results in TGF-β1 signalling downregulation, decreased fibroblast activity and collagen synthesis, improving the intratumoural penetration of therapeutics.[14–16]

We evaluated losartan as a potential mechanism to reduce collagen accumulation in the matrix of the PDAC cultures and improve interstitial flow to increase gemcitabine delivery to the cancer cells. With losartan treatment, our microfluidic PDAC culture resulted in reduced collagen amounts, improved hydraulic conductivity of the model's interstitial space and gemcitabine efficacy. The results presented show how important it is to have appropriate 3D replication of the *in vivo* biophysical hallmarks for cancers such as PDAC for adequate drug studies.

## Experimental section

### Microfluidic device design and fabrication

A 5-channel microfluidic device was designed using Autodesk's AutoCAD® software and fabricated using photolithography and PDMS soft lithography. Fig. 1A shows a CAD schematic of the

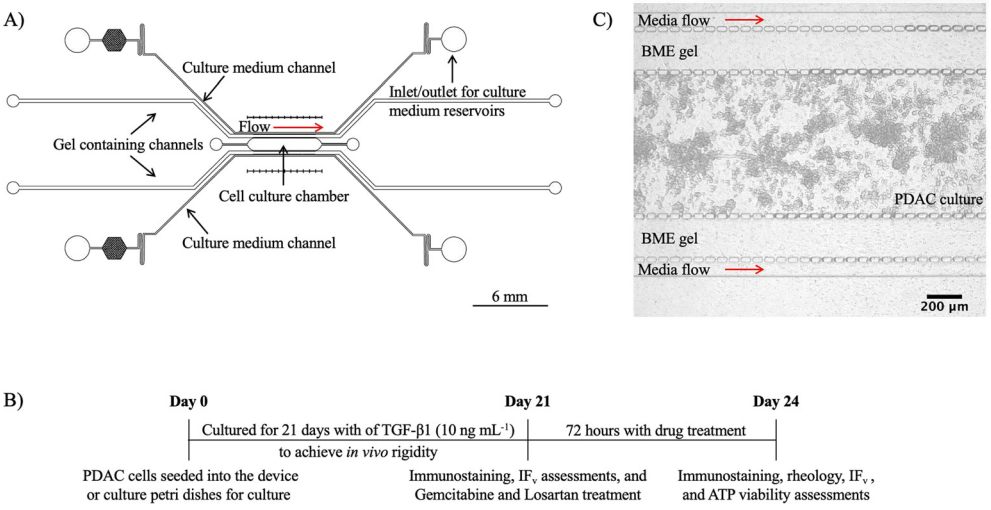


**Fig. 1** A) CAD of the 5-channel microfluidic device used for growing the PDAC culture model (PANC-1 : PSC co-culture in a 1 : 3 ratio with 10 ng $mL^{-1}$ of TGF-β1 supplement). The device consists of a central culture chamber, two gel containing channels, and two media channels. B) Timeline of the seeding of the PDAC (PANC-1 and PSC, 1 : 3 seeding ratio) cells for a 21-day culture. With mechanical maturity achieved by day 21, the cultures were treated with gemcitabine only, losartan only, or gemcitabine and losartan together for 72 hours before ATP viability assessment. Immunostaining for collagen and HIF-1 alpha, oscillatory shear rheology, and interstitial flow were also assessed following treatment. C) The microfluidic PDAC culture 24 hours after seeding. Scale bar 200 μm.

device. Topographically, the 5-channel microfluidic device consisted of a 1 mm × 6 mm ($w \times L$) culture chamber, two 275 μm wide gel containing channels, and two 100 μm wide media channels adjacent to the gel containing channels. At the boundary of the channels, micropillars with a 5 μm interspace were included to help confine cells and gels in the respective channels and for the stable diffusion of medium into the culture chamber to grow our PDAC model.

Photolithography was used to make an SU-8 master silicon wafer mould of the CAD. A 4-inch silicon wafer was coated with SU-2075 negative photoresist (Microchem, Newton, MA) for a device depth of 100 μm. The CAD of the device was exposed onto the SU-2075 coated silicon wafer with a direct write laser (MicroWriter™, Durham Magneto Optics, Durham, UK) at a laser power of 375 nm and a resolution of 2 μm. For moulding into a solid substrate, base PDMS and cross-linking agent (Sylgard™ 184 Silicon Elastomer Kit) were mixed at a weight ratio of 10 : 1. The mixture was degassed for 1 hour under vacuum at room temperature, poured onto the silicon wafer mould, and cured for at least 1 hour at 72 °C. After curing, the PDMS moulds were cut out, and the inlets and outlets were formed using a 1 or a 2 mm diameter biopsy punch. The PDMS moulds were then bonded onto PDMS-coated (50 μm thick) glass slides using $O_2$ plasma and placed in an oven for at least 1 hour. The devices were autoclaved prior to cell culture.

### Cell lines and culture

Pancreatic ductal adenocarcinoma cells, PANC-1 (ECACC 87092802),[17] were maintained in DMEM (ThermoFisher Scientific)/10% FBS (Sigma Aldrich) culture medium supplemented with 1% penicillin streptomycin (P/S; Sigma-Aldrich) and 1% GlutaMAX (Thermo Fisher Scientific). Human pancreatic stellate cells (PSCs) were maintained in stellate cell medium supplemented with 10% FBS, 1% stellate cell growth supplement, and 1% P/S in culture flasks coated with poly-L-lysine (10 mg $mL^{-1}$) overnight. PSCs and their culture reagents were sourced from ScienCell™ Research Laboratories supplied by Caltag Medsystems Ltd. The PANC-1 and PSC cell cultures were maintained at 37 °C with 5% $CO_2$ under humidified conditions (95–99%). The cells were passaged with TrypLE Express Enzyme (1×) with no phenol red (ThermoFisher Scientific) once ≥70% confluence was achieved.

### Microfluidic PDAC culture

$1 \times 10^6$ cells $mL^{-1}$ of PANC-1 and PSC cells in a 1 : 3 seeding ratio was mixed with 6–9 mg $mL^{-1}$ of Cultrex® Basement Membrane Extract (BME) gel (R&D systems, Bio-Techne) to provide a scaffold for the 3D cell culture of the cells. The mixture was pipetted into the 5-channel device culture chamber and incubated at 37 °C with 5% $CO_2$ under humidified conditions for approximately 30 minutes. After incubation, 9–12 mg $mL^{-1}$ BME gel was pipetted into the gel containing channels. This was followed by another 30 minutes of incubation to polymerise the gel. Fluid reservoirs[18] were then inserted into the respective inlets and outlets of the device culture media channels, and the cells were grown with DMEM/10% FBS medium supplemented with TGF-β1 supplement (10 ng $mL^{-1}$; Sigma-Aldrich) for 21 days at 37 °C with 5% $CO_2$ under humidified conditions.

Culture viability, with increased culture time, was investigated with ReadyProbes™ Cell Viability Imaging Kit, Blue/Red (ThermoFisher Scientific). Drops of NucBlue™ Live (Hoechst stain) and propidium iodide were added to the culture medium in the fluid reservoirs for incubation. After incubation, the cultures were imaged with a Leica-TCS-SP8 confocal laser scanning microscope using a 10× objective and a pinhole of 1.00 AU with the respective excitation and emission wavelength of the stains. Acquired images were analysed with ImageJ.

### PDAC culture in BME gel

Like the *PDAC Spheroid Culture with an ECM Environment* as described previously,[13] $1 \times 10^6$ cells $mL^{-1}$ of PANC-1 and PSC cells (1 : 3 seeding ratio) were seeded into 21.5 $cm^2$ Nunclon Delta surface treated cell culture Petri dishes (Thermo Fisher Scientific) with 6–9 mg $mL^{-1}$ of BME gel. The gel was used as a scaffold for 3D cell culture, which appeared spherical. The PANC-1 : PSCs (PDAC) cells were grown with DMEM/10% FBS medium supplemented with TGF-β1 supplement (10 ng $mL^{-1}$) under humidified conditions at 37 °C with 5% $CO_2$ up to 21 days to investigate the PDAC culture mechanical stiffness and the presence of collagen by immunostaining following treatment with losartan.

### Oscillatory shear rheology of the PDAC cultures in BME gel

Oscillatory shear rheology was used to measure the complex shear modulus, the mechanical stiffness, of the PDAC cells grown in BME gel for 21 days, as previously described.[13] ESI† Fig. S1A shows the set-up of the cultures for the rheological assessment. Briefly, replicate cultures of the PDAC cells seeded into cultures dishes with BME gel for a 21-day 3D off-chip culture in hydrogel (as described in *PDAC culture in BME gel* above) were taken from the cell culture incubator and placed on the bottom plate of an Anton Paar MCR 302 stress-controlled rheometer. A 50 mm parallel plate geometry, with anti-slip material to prevent sample slippage, was brought into contact with the cultures in the culture dishes at a working gap between 0.5–1 mm. Pseudo-strain-controlled shear deformation time sweeps were performed at a shear strain of 2% strain (strain ramp measurements, ESI† Fig. S1B, show a reasonably linear viscoelastic region up to ≈5% strain) and frequency of 0.5 Hz for 600 seconds. Frequency sweep measurements from 0.01–100 Hz, with a constant shear strain of 2%, were performed to determine the time-dependent structural behaviour of the cultures under deformation. After the oscillatory shear deformation, the 50 mm parallel plate geometry was released from contact with the cultures. The cultures were removed from the bottom

 

plate of the rheometer for disposal. Eqn (1) defines the complex shear modulus

$$G^* = G' + iG'' \quad (1)$$

where $G'$ and $G''$ components are the elastic or storage and viscous or loss moduli measurements, respectively. $G^*$ is the complex shear modulus. All units are in Pascal (Pa). As biological samples, *i.e.*, cell and tissue cultures, are viscoelastic (neither purely elastic nor purely viscous), the complex sum of $G'$ and $G''$ provides information on the extent to which the sample can resist deformation, the mechanical stiffness ($G^*$).[19–21]

### Immunostaining of the PDAC cultures in BME gel for collagen, actin, and HIF-1 alpha

The PDAC cells, grown in BME gel for up to 21 days and treated with and without losartan, were fixed with formaldehyde 4% aqueous solution (VWR) for 30 minutes at room temperature. After fixation, the cultures were permeabilised with 0.2% Triton X-100 (Sigma Aldrich) in 1% BSA (Sigma Aldrich) and 5% FBS (Sigma Aldrich) solution for 1 hour at room temperature. The cultures were incubated with recombinant anti-collagen I antibody and recombinant anti-HIF 1 alpha antibody overnight at 4 °C and followed with secondary antibody, goat anti-rabbit Alexa Fluor™ 488, for 1 hour at room temperature. All antibodies were prepared in 1 mL PBS containing 1% BSA. Actin was stained with phalloidin-iFluor 647. The antibodies and actin stain were sourced from Abcam. Nuclei were stained with DAPI (Boster Biological Technology). The PDAC cultures were then imaged with the respective excitation and emission wavelength of the stains according to the manufacturer's instructions using the Leica confocal fluorescence microscope with a 10× objective and a pinhole of 1.00 AU. The acquired images were analysed with Image J.

### Immunostaining of the microfluidic PDAC cultures for collagen, actin, and HIF-1 alpha

All reagents were introduced into the device with the cultures *via* the culture media channels using fluid reservoirs. The cultures were washed with PBS for 10 minutes, fixed with formaldehyde 4% aqueous solution (VWR) and permeabilised with 0.2% Triton X-100 (Sigma Aldrich) in 1% BSA (Sigma Aldrich) and 5% FBS (Sigma Aldrich) solution for up to 15 minutes at room temperature. The cultures were then incubated with recombinant anti-collagen I antibody (rabbit monoclonal [EPR22894-89] to collagen I) and recombinant anti-HIF 1 alpha antibody (rabbit monoclonal [EPR16897] to HIF-1 alpha) for up to 1 hour at room temperature. Secondary antibody staining was performed with goat anti-rabbit Alexa Fluor™ 488 (ab150077) for 1 hour at room temperature. Actin was stained with phalloidin-iFluor 647. The nuclei were stained with DAPI (Boster Biological Technology). All antibodies were prepared in 1 mL PBS containing 1% BSA. The antibodies and actin were sourced from Abcam. The immunostained microfluidic cultures were imaged with the Leica confocal fluorescence microscope using a 10× objective and a pinhole of 1.00 AU with the respective excitation and emission wavelength of the stains according to the manufacturer's instructions. All acquired images were analysed with Image J.

### Interstitial flow assessment of the microfluidic PDAC cultures

Interstitial flow was assessed by investigating the hydraulic conductivity of the interstitial space of the culture environment. The interstitial flow was described with Darcy's law as[22]

$$\mathrm{IF}_v = -K\nabla P \quad (2)$$

where $\mathrm{IF}_v$ is the interstitial fluid velocity (μm $s^{-1}$), $K$ is the hydraulic conductivity ($m^2$ $s^{-1}$ $Pa^{-1}$), and ∇P is the pressure gradient (Pa) (from differences in flow velocities in the media channels) driving fluid transport through the culture interstitial space.

To investigate the interstitial flow of the culture model and to accurately create a pressure gradient across the culture chamber with the model, a syringe pump was used to perfuse carboxyfluorescein in DMEM/10% FBS medium in a 1 : 10 ratio (referred to as fluorescein-media solution) into the device with the culture model. Two 1 mL glass syringes (SGE gas-tight syringes Luer Lock, Sigma Aldrich) were loaded with the fluorescein-media solution or culture medium only for perfusion at a flow rate of 0.5 and 0.1 μL $min^{-1}$, respectively. The time taken for the fluorescein-media solution to permeate through the microfluidic PDAC culture was determined. Shear stress induced in the media channels and in the culture chamber was approximated with the wall-shear model for a rectangular channel[23,24] using

$$\tau = \frac{6\mu Q}{wh^3} \quad (3)$$

where $\tau$ is the shear stress (Pa) converted into dyne $cm^{-2}$, $\mu$ is the dynamic viscosity of the culture medium, $Q$ is the volumetric fluid flow rate ($m^3$ $s^{-1}$), and $w$ and $h$ is the width and depth of the culture channel in metres, respectively.

### Gemcitabine only assessment

Gemcitabine (Sigma Aldrich) was dissolved to a 5 mg $mL^{-1}$ stock concentration with DMSO (Sigma Aldrich) and diluted with DMEM/10% FBS medium to assess its effect on the microfluidic PDAC cultures. The cultures were treated with 31.25 μM of gemcitabine for 72 hours. After the 72-hour incubation with gemcitabine, ATP viability was assessed by quantifying the ATP content with CellTiter-Glo® 3D cell viability assay (Promega). According to the manufacturer's instructions, a volume of CellTiter-Glo reagent, equal to the volume of culture medium present in the fluid reservoir with the microfluidic cultures, was added for incubation. After incubation, the effluent in the fluid reservoir and the whole

on-chip culture in the culture chamber were removed by pipetting into opaque plates for luminescence reading with a microplate reader (SpectraMAX M2, Molecular Devices). Viability was normalised to positive and negative controls.

### Losartan only assessment

Losartan (Biotechne, Tocris) was dissolved in DMSO (Sigma Aldrich) to a stock concentration of 46.1 mg $mL^{-1}$ and diluted with DMEM/10% FBS medium to assess its effect on the PDAC cultures – off-chip with BME gel and the microfluidic PDAC culture model. The PDAC cultures were treated with 0, 1, 10, 50, and 100 μM of losartan for 72 hours. ATP viability was assessed with the CellTiter-Glo® 3D cell viability assay, where a volume of CellTiter-Glo reagent equal to the volume of culture medium present in the Petri dishes and fluid reservoir was added. The cultures were then incubated with the reagent, and the whole cultures were transferred by pipetting into opaque plates for luminescence reading with a microplate reader. Culture viability was normalised to positive and negative controls.

### Gemcitabine and losartan treatment together

Gemcitabine and losartan were solubilised in DMSO to a stock concentration of 5 mg $mL^{-1}$ and 46.1 mg $mL^{-1}$, respectively, and diluted together in DMEM/10% FBS medium to a final concentration of 31.25 μM gemcitabine and 10 μM losartan. This was used to treat the 21-day microfluidic PDAC cultures for 72 hours. Viability was performed with the CellTiter-Glo® 3D cell viability assay as described above and normalised to positive and negative controls to determine the efficacy of gemcitabine with losartan treatment.

### Statistical analyses

Data were expressed as mean ± standard error (SE) for biological and experimental repeat, and using OriginPro software, statistical significance was assessed. Normality and equal of variance were tested, and once normality and equality of variance assumptions were satisfied, significance was measured with one-way ANOVA, followed by Tukey's multiple comparisons test. $p \leq 0.05$ was considered statistically significant.

## Results and discussion

The rigid collagen-rich tumour microenvironment with reduced interstitial flow underlines the poor therapeutic efficacy and dismal prognosis of PDAC.[8] We have previously demonstrated off-chip how the PDAC stroma impacts drug effect.[13] We showed how PANC-1 and PSCs co-culture with TGF-β1 supplement triggers collagen production for increased mechanical stiffness and poor gemcitabine efficacy. This demonstrated that our PDAC culture could be used to evaluate novel therapeutics against PDAC cells. Nonetheless, despite having a mechanical rigidity within range of the mechanical stiffness of the PDAC tumour tissue[21,25] with a 21-day growth, the culture was developed in a static well plate format, lacking the hydraulic environment and transport properties present in tumour tissues in the body.

### The microfluidic device and the microfluidic PDAC culture model

With the aim of building a relevant PDAC culture model with microphysiological flow conditions for drug studies, a 5-channel microfluidic device was fabricated and used for growing PDAC cells for 21 days. The growing of the cells for 21 days was to mimic the PDAC tumour microenvironment and rigidity. PDAC cells were seeded with BME hydrogel to provide a scaffold for the 3D cell culture in our microfluidic device, and from day 7 to 21 of culture, there was an increase in cell population and matrix engineered by the cells with collagen production. Fig. 1A shows the CAD of the 5-channel microfluidic device used for the 21-day PDAC model. The PDAC model consisted of the cancer cells PANC-1, the pancreatic fibroblast cells, PSCs, and TGF-β1 (10 ng $mL^{-1}$) supplement. The 5-channel microfluidic device was made in-house using photolithography and PDMS soft-lithography. For long-term cell culture to achieve the stroma environment and rigidity of the PDAC tumour tissue, gel-only containing channels were placed between the culture chamber and the media channels to prevent cells from the central culture chamber from growing into the media channels and obstructing flow over the 21-day culture period. Fluid reservoirs were used to introduce cell media *via* hydrostatic pressure into the device for culture, mimicking *in vivo* physiological flow conditions and eliminating issues with the use of a syringe pump and tubing for perfusion culture.[18,26]

Our microfluidic PDAC culture model recapitulated the collagenous, hypoxic PDAC tumour microenvironment with reduced interstitial flow for assessment with gemcitabine and losartan treatment. Losartan's mechanism of action in reducing high blood pressure is *via* the renin-angiotensin-aldosterone system (RAAS). RAAS plays a role in collagen production *via* TGF- β1 signalling pathway, and losartan reduces collagen production *via* RAAS by downregulating TGF-β1 activators such as TSP-1.[14] As a result, losartan was used to reduce the levels of collagen and improve interstitial flow in our model to investigate the efficacy of gemcitabine. After treatment with losartan, collagen deposition, culture stiffness, hydraulic conductivity, and gemcitabine efficacy were evaluated.

Prior to assessments with gemcitabine and losartan, culture viability of the developing model was performed, and culture mechanical assessment was performed with oscillatory shear deformation to investigate culture stiffness. Immunostaining for collagen and HIF-1 alpha were performed to determine the development of a collagenous hypoxic environment, and hydraulic conductivity assessments were performed to investigate the effect of the collagenous environment on interstitial flow. Fig. 1B shows a timeline of the seeding of the PDAC cells for a 21-day culture, followed by the different

 

assessments and treatments with gemcitabine and losartan. Fig. 1C shows a bright-field image of the PDAC cells in the culture chamber of the 5-channel device 24 hours after seeding.

Viability assessment of the developing microfluidic culture model showed the model to be live and viable over 21 days. Fig. 2A shows the live/dead stain and ATP viability assessment of the microfluidic PDAC model over the 21-day culture period. Live/dead viability assessment consisted of NucBlue® Live (Hoechst stain) to stain the nucleus of live cells and propidium iodide (PI), which binds to the DNA of dead cells to fluoresce red. There were minimal dead cells with less PI staining in comparison to the Hoechst stain, showing qualitatively that the cultures were viable. Few dead cells were observed, mostly around the gel containing channels and media channels. This could be due to the shear stress imposed with a culture medium flow of 0.5 μL $min^{-1}$

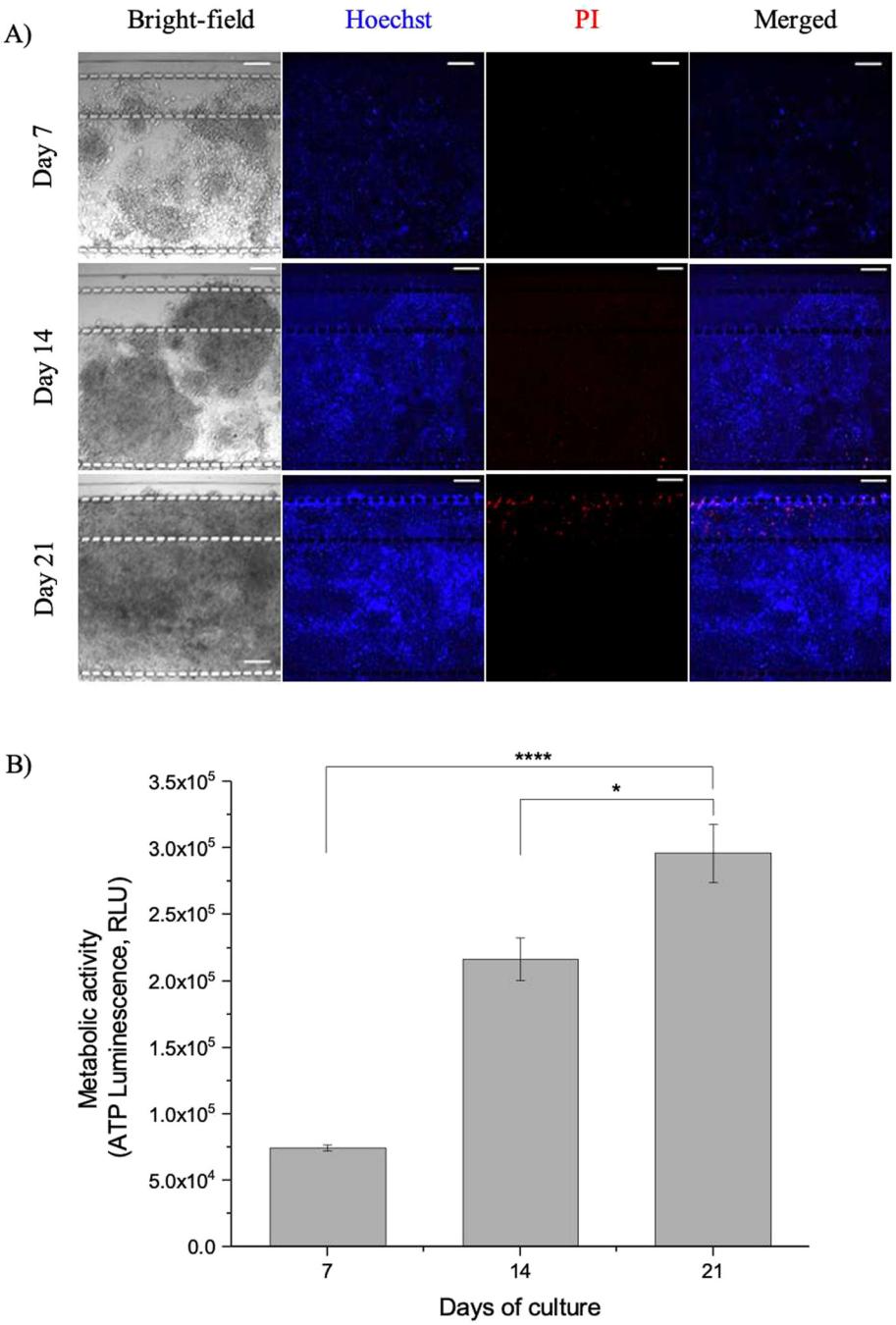


**Fig. 2** A) Confocal images of the live/dead viability assessment of the growing microfluidic PDAC culture model on days 7, 14, and 21 of culture with Hoechst (in blue) for live cells and propidium iodide (PI; in red) for dead cells. Scale bar, 200 μm. B) ATP viability assessment of the growing model on days 7, 14, and 21 of culture, where $n$ = 18 devices per day of culture generated from three separate seeding settings. ****$p < 0.0001$ and *$p < 0.5$, one-way ANOVA followed by Tukey's multiple comparison test.

in the media channels. The shear stress in the media channels, with a flow rate of 0.5 μL $min^{-1}$, was 0.35 dyne $cm^{-2}$. This was low compared to the physiological shear stress, which ranges between 0.5–120 dyne $cm^{-2}$ for blood and lymphatic vessels and tissues.[26] However, this was enough to induce shear forces on the few cells proximal to the media channels, affecting their viability.

The live/dead staining viability assessment of the cultures was in line with the quantitative assessment of the viability of the cultures. Fig. 2B shows the ATP metabolic activity of the microfluidic PDAC model. There was increased ATP luminescence proportional to the ATP concentrations in the cultures, with increased culture time. This showed the microfluidic model was viable and growing in the culture chamber over the 21 days. ESI† Fig. S2 shows a representative confocal *z*-stack image with PANC-1 cell-only culture to assess the growth of the PDAC culture model in the entire depth of the microfluidic culture chamber.

### The matrix environment and the effect on interstitial flow

Fig. 3 shows immunostained images of the microfluidic PDAC model for collagen type I (in green) as it developed mechanically. DAPI (in blue) was used to stain the cell nucleus, and phalloidin (in red) was used to stain f-actin for the cell cytoskeletal structure. ESI† Fig. S3A shows negative control images of PDAC cultures grown in BME immunostained for collagen type I prior to immunostaining the microfluidic PDAC model. Immunostaining of the model for collagen type I showed how the PDAC cells build a collagenous matrix environment with increased culture time. There was increased collagen in the matrix environment of the day 21 microfluidic PDAC model compared to days 7 and 14 of culture. On days 7 and 14 of culture, collagen accumulation was observed in and around the cells but not in the surrounding culture matrix. This observation was in line with the previous assessment of our off-chip PDAC cultures and their subsequent measured mechanical stiffness, where on days 7 and 14 of culture, there was decreased complex shear modulus and collagen seen mostly at the culture periphery and increased complex shear modulus with collagen observed in the matrix by day 21 of culture. This shows the microfluidic PDAC culture had started to mimic the collagenous PDAC tumour microenvironment and, therefore, stiffness.[13]

Beer *et al.* 2017, Bradney *et al.* 2020, Drifka *et al.* 2013, and Lee *et al.* 2018 presented microfluidic cultures of pancreatic cancer cells embedded in a collagen matrix and cultured for 5–10 days to study the effect of stroma-cancer interactions and epithelial-mesenchymal transition (EMT) on therapeutic efficacy.[27–30] A 5–10 days culture, compared to our previous assessments and as seen here in Fig. 3, indicated the PDAC tumour mechanics, with cells building their own natural mechanically stiff matrix environment, would not be taken into account. Here, the PDAC cells were seeded with BME gel for the cells to naturally develop mechanically with the production of essential structured proteins (*i.e.*, collagen) to support their growth and mimic the biophysical cues of the tumour microenvironment.[31,32] If our microfluidic cultured PDAC cells were grown for 5–10 days, the stiffness achieved would be <300 Pa, and the culture would be mechanically immature, with little

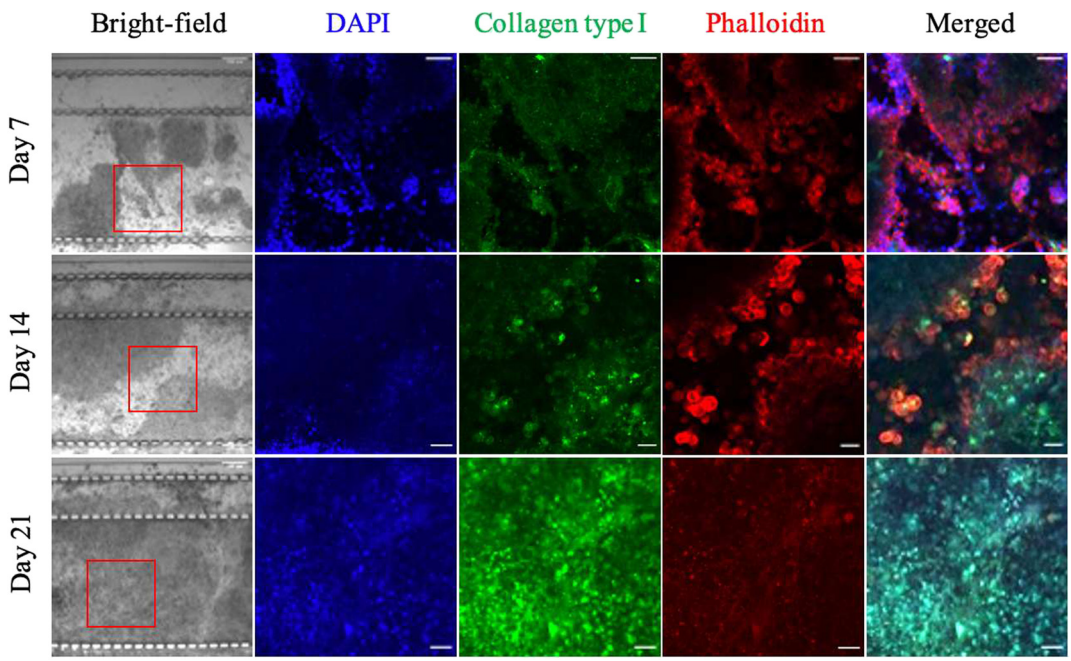


Fig. 3 Confocal images of the immunostained microfluidic PDAC culture model for collagen type I in green on days 7, 14, and 21 of culture. Nuclei stained with DAPI in blue, collagen type I stained in green, and actin with phalloidin in red. DAPI, collagen, phalloidin, and merged images are magnified images of the red box in the bright-field images. Scale bar for bright-field images, 200 μm. Scale bar for magnified images on day 7, 100 μm. Scale bar for magnified images on days 14 and 21 of culture, 50 μm.

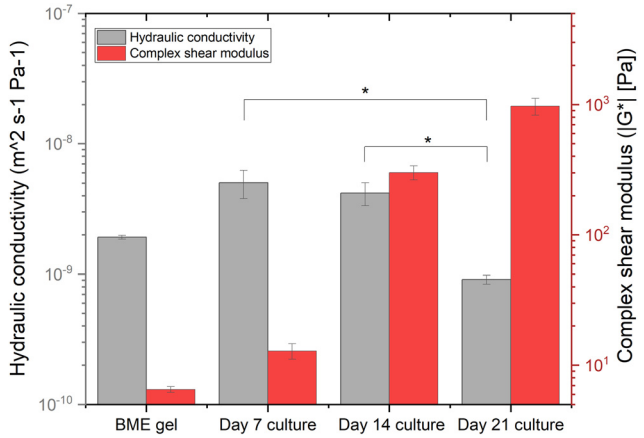


**Fig. 4** The hydraulic conductivity of the interstitial space of the BME gel only and the microfluidic PDAC culture model on days 7, 14, and 21 of culture with the perfusion of the fluorescein-media solution, compared to their respective complex shear modulus[13] $N$ = 3–4 devices for the BME gel only and the microfluidic PDAC model per day of culture generated from three separate seeding settings. * $p < 0.05$, one-way ANOVA followed by Tukey's multiple comparison test.

collagen seen in the culture matrix.[13] Moreover, the model will not exhibit reduced interstitial flow, as is observed *in vivo*.[33–36]

Determining how the collagenous matrix affected the culture interstitial flow, the hydraulic conductivity of our PDAC model was assessed. The interstitial flow was investigated with a fluorescein-media solution. As a control, the perfusion of the fluorescein-media solution was assessed with 6–9 mg mL$^{-1}$ BME gel only. ESI† Fig. S4 shows images of the perfusion flow and the plot of the fluorescein intensity *versus* the distance travelled by the solution over time. Compared to the flow of the fluorescein-media solution through the BME gel only, it took >90 minutes for the intensity of the fluorescein-media solution to be homogenous throughout the culture chamber of our 21-day PDAC model. This was due to the reduced hydraulic conductivity of the culture interstitial space with increased collagen.

Kramer *et al.* 2019 and Lai *et al.* 2020 investigated the interstitial flow nature of their PDAC cultures grown in an OrganoPlate and InVADE chip, respectively, by evaluating with time-lapse imaging the movement of tetramethyl rhodamine isothiocyanate (TRITC)-dextran and carboxyfluorescein diacetate (CFDA), respectively.[37,38] Kramer *et al.* report their high interstitial flow speed to be within *in vivo* range and resulting in decreased cell proliferation due to lack of nutrients. These results are quite surprising as increasing intratumoural pressure from an increasingly dense stroma microenvironment leads to decreased interstitial flow, which results in limited access of nutrients to cells, affecting cell proliferation. The reduced cell proliferation observed by Kramer *et al.* could be due to the high shear stress imposed on the cells with the high flow speed.[39] While these platforms undoubtedly show an advancement in PDAC disease modelling, the cultures presented did not include fibroblasts or cancer-associated fibroblast (CAF) cells resulting in the lack of an adequate tumour stroma microenvironment to assess interstitial flow. Also, the OrganoPlate used for their cultures was based in a well plate format, requiring a mechanical rocking platform to induce flow.[38] This shows the cultures did not represent the PDAC tumour microenvironment, and the cultures were grown in well conditions, lacking a differential pressure gradient to adequately investigate interstitial flow. Lai *et al.* found a decrease in the movement of the CFDA solution through areas of their cultures, which included fibroblasts with high collagen accumulation.[37] However, the InVADE chip used was also based in a static well format as opposed to the advantage of a perfusion culture to simulate the hydraulic flow conditions in tumour tissues. Also, they did not use fibroblasts native to the PDAC tumour tissue, which can influence the genetic and phenotypic behaviour of their cultures.[40,41]

Fig. 4 and Table 1 show data on interstitial flow with the hydraulic conductivity assessment of the interstitial space of our developing microfluidic PDAC culture model. As a control, the hydraulic conductivity of BME gel only in the culture chamber of our device was investigated. The percentage decrease in the hydraulic conductivity of the interstitial space of the 21-day culture, compared to the interstitial space on days 7 and 14, was approximately 82% and 78%, respectively. The mechanical stiffness of the PDAC culture on days 7 and 14 was 12.84 ± 1.74 Pa and 301.19 ± 36.36 Pa, respectively, as a result of the cells breaking down their surrounding matrix and producing ECM proteins, including collagen, into their environment.[13,42] This resulted in the increased interstitial flow compared to the 21-day culture, which exhibited increased collagen content and mechanical stiffness of approximately 1 kPa. By day 21 of culture, when the PDAC cells developed a collagenous matrix

**Table 1** The interstitial flow assessment of the microfluidic PDAC culture model. The hydraulic conductivity, interstitial flow velocity, and shear stress with the perfusion of fluorescein-media solution in the culture chamber with the PDAC model or 6–9 mg mL$^{-1}$ BME gel only. $N$ = 3 or 4 per culture condition from three separate seeding settings

| Culture sample | $K_s$ [m$^2$] | $K'$ [m$^2$ s$^{-1}$ Pa$^{-1}$] | IF$_v$ [μm s$^{-1}$] | $\tau$ [dyne cm$^{-2}$] |
|---|---|---|---|---|
| BME gel only | $1.3 \times 10^{-12} \pm 4.4 \times 10^{-14}$ | $1.9 \times 10^{-9} \pm 6.3 \times 10^{-11}$ | $6.3 \times 10^{-4} \pm 2.1 \times 10^{-5}$ | $2.6 \times 10^{-8} \pm 8.7 \times 10^{-10}$ |
| Day 7 culture model | $3.5 \times 10^{-12} \pm 8.5 \times 10^{-13}$ | $5.0 \times 10^{-9} \pm 1.2 \times 10^{-9}$ | $1.6 \times 10^{-3} \pm 4.1 \times 10^{-4}$ | $6.9 \times 10^{-8} \pm 2.3 \times 10^{-8}$ |
| Day 14 culture model | $2.9 \times 10^{-12} \pm 5.8 \times 10^{-13}$ | $4.2 \times 10^{-9} \pm 8.4 \times 10^{-10}$ | $1.4 \times 10^{-3} \pm 2.7 \times 10^{-4}$ | $5.8 \times 10^{-8} \pm 1.2 \times 10^{-8}$ |
| Day 21 culture model | $6.3 \times 10^{-13} \pm 4.8 \times 10^{-14}$ | $9.1 \times 10^{-10} \pm 6.9 \times 10^{-11}$ | $3.0 \times 10^{-4} \pm 2.3 \times 10^{-5}$ | $1.2 \times 10^{-8} \pm 9.6 \times 10^{-10}$ |
| Day 21 culture model with 10 μM losartan | $1.01 \times 10^{-12} \pm 1.9 \times 10^{-13}$ | $1.46 \times 10^{-9} \pm 2.8 \times 10^{-10}$ | $4.8 \times 10^{-4} \pm 9.2 \times 10^{-5}$ | $2.01 \times 10^{-8} \pm 3.8 \times 10^{-9}$ |

$K_s$, specific hydraulic conductivity; $K'$, hydraulic conductivity; IF$_v$, interstitial flow velocity; $\tau$, shear stress.

environment, there was a reduction in the interstitial flow across the culture chamber, resulting in the reduced hydraulic conductivity. ESI† Videos S1 and S2 show the fluorescein-media solution flow through the 21-day microfluidic PDAC model and BME gel only, respectively.

Interstitial flow is an important mechanism for the delivery of nutrients, oxygen, and drugs to cells and for the removal of waste. A reduction in interstitial flow results in a hypoxic and acidic environment from limited access to nutrients and oxygen and the removal of waste, with HIF-1 alpha orchestrating the metabolic switch for cells to survive in this environment.[43–45] HIF-1 alpha is a transcription factor that is central to cellular response to low oxygen levels, shifting metabolic activity from oxidative phosphorylation to glycolysis to allow cells to survive.[46–48] Therefore, the presence of a hypoxic environment was investigated by immunostaining the microfluidic PDAC model for HIF-1 alpha. Fig. 5 shows immunostained images of the 21-day microfluidic PDAC culture expressing HIF-1 alpha. The nucleus and cytoskeletal structure of the cells were also stained with DAPI in blue and phalloidin in red, respectively. ESI† Fig. S3B shows negative control images of PDAC cultures grown in BME gel immunostained for HIF-1 alpha prior to immunostaining the microfluidic PDAC model. The expression of HIF-1 alpha was consistent with off-chip observations, where on day 21 of culture, with a rigid collagenous matrix, the model exhibited a hypoxic microenvironment.[13] In a hypoxic and acidic environment, there is the upregulation of lysyl oxidase proteins, resulting in excess production and cross-linking of fibrous proteins (*i.e.*, collagen) for a fibrotic rigid stroma. This correlates to overall poor survival as a result of ineffective therapeutic delivery to the cancer cells.[49,50]

### Losartan decreases matrix collagen content and mechanical stiffness in a dose-dependent manner

With our microfluidic PDAC model mimicking the PDAC tumour's rigid collagenous matrix environment with reduced interstitial flow, we tested how the use of the matrix-depleting drug, losartan, will affect collagen deposition, culture stiffness and interstitial flow. The penetration of drugs into fibrotic tumours has been investigated with matrix modifiers such as collagenase, relaxin, and matrix metalloproteinases.[14,51] These have been shown to modify the fibrous and proteoglycan network in tumours improving the efficacy of drugs. However, these drugs result in toxicity effects with the risk of increased tumour progression.

Losartan, an anti-hypertensive drug, has been shown to inhibit collagen synthesis and reduce cardiac and renal fibrosis in orthotopic mouse models, improving the intratumoural distribution and efficacy of nanoparticles with limited side effects.[14,52] As such, we hypothesised that losartan would reduce the collagen levels in our 21-day microfluidic PDAC culture model, improve interstitial flow and, thus, drug efficacy. First, different losartan concentrations were tested on off-chip PDAC cultures. This was to determine an optimum losartan concertation (resulting in decreased collagen levels, increased interstitial flow, and percentage viability providing room to assess further viability decreases with other therapeutics) for our culture model. PDAC cells were seeded into culture Petri dishes and cultured for 21 days for a 72-hour incubation with 1, 10, 50, and 100 μM losartan. After 72 hours, the cultures were fixed and immunostained for collagen type 1, and their mechanical stiffness was assessed with oscillatory shear rheology. Fig. 6A shows the immunostained images for collagen type I (in green) with the different losartan concentrations. DAPI (in blue) was used to stain cell nuclei, and phalloidin (in red) was used to stain the cell cytoskeleton.

With increasing losartan concentration, there was a reduction in the levels of collagen in the cell culture microenvironment. Increased losartan concentration also corresponded to decreased culture mechanical stiffness (complex shear modulus) by ~43% (520 ± 185 with 10 μM losartan *vs.* 904 ± 36 with 0 μM losartan) with decreased elastic (storage) and viscous (loss) moduli components. Fig. 6B shows the shear moduli measurements of the cultures with increased losartan concentration. Collagen, a fibrous protein, provides the basic mechanical framework of the ECM architecture,[53–55] underlining tissue elasticity and strength. Losartan attenuates the TGF-β1 signalling pathway and activity of the PSCs in producing abundant ECM fibrous proteins, resulting in decreased levels of collagen and, thus, culture elasticity and mechanical stiffness.[15,52]

The decreased culture viscosity was likely due to a decrease in the gel-fluid phase with gelatinous matrix macromolecules

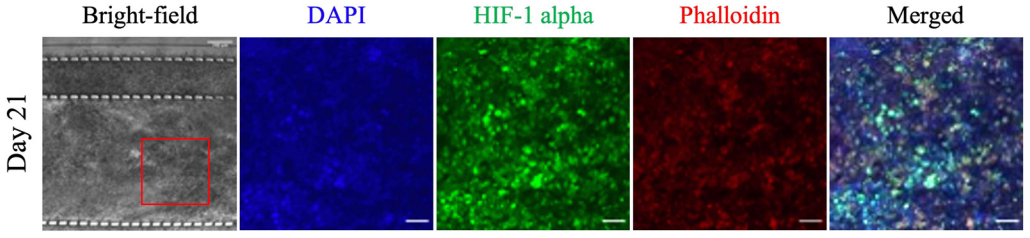


Fig. 5 HIF-1 alpha on day 21 of culture. Nuclei stained with DAPI in blue, HIF-1 alpha in green, and actin with phalloidin in red. DAPI, HIF-1 alpha, phalloidin, and merged images are magnified images of the red box in the bright-field images. Scale bar for bright-field images, 200 μm. Scale bar for magnified images, 50 μm.

 

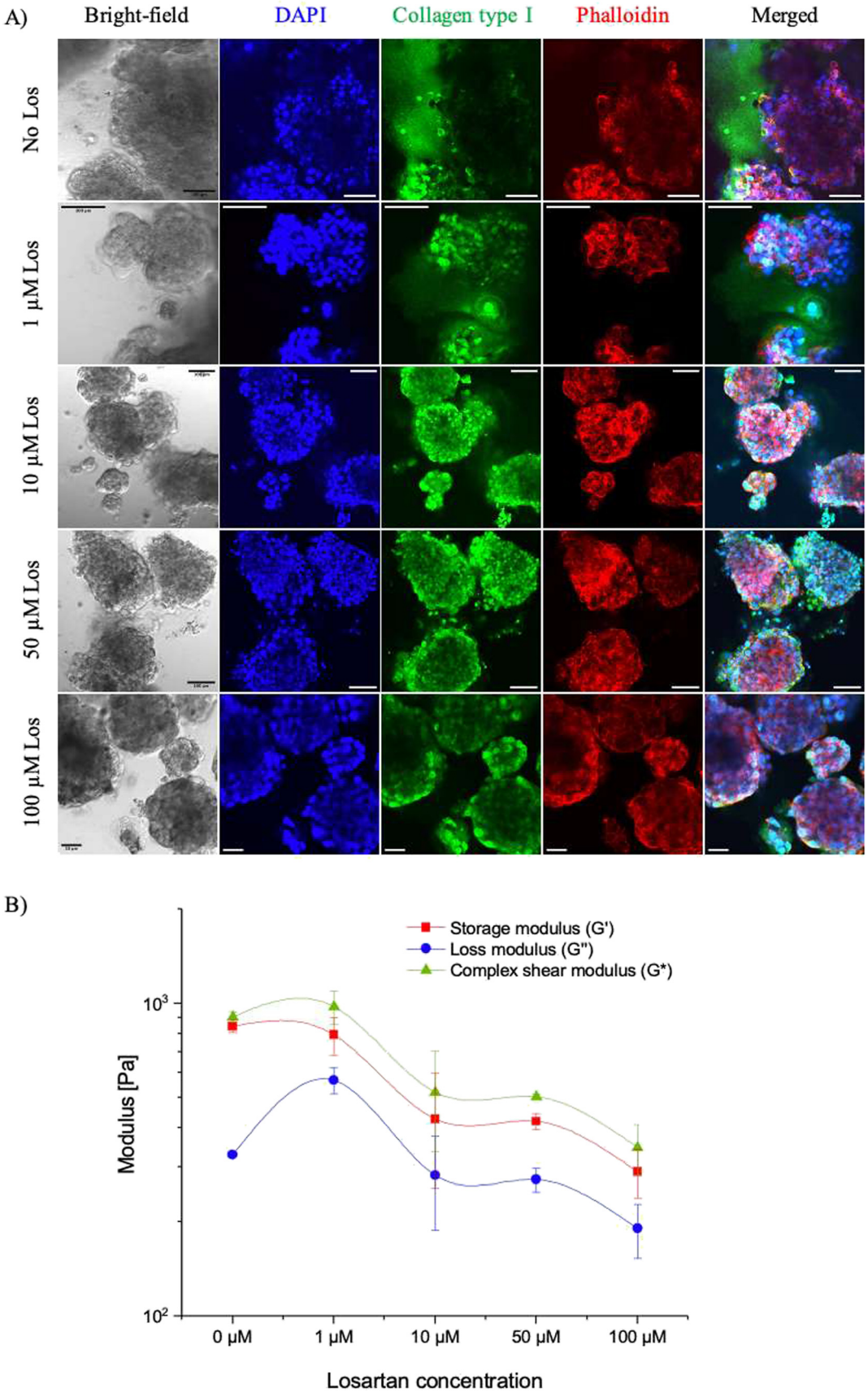


**Fig. 6** A) Confocal images of the immunostained 21-day off-chip PDAC culture for collagen type I in green following treatment with losartan of different concentrations. The nuclei and phalloidin of the cultures were stained with DAPI (in blue) and phalloidin (in red), respectively. Scale bar is 100 μm and 50 μm for the 100 μM losartan treated cultures. B) The storage (or elastic), loss (or viscous), and complex shear moduli of the 21-day off-chip PDAC cultures treated with losartan of different concentrations. *N* = 3 culture plates per culture day.

such as hyaluronan, which, in addition to collagen, contributes to the solid stress in tumours.[1,52] Losartan has been shown to reduce the production of hyaluronan.[52] Hyaluronan is a glycosaminoglycan which plays a role in cellular processes, including cell adhesion, migration, and proliferation.[56] It has been shown to accumulate in the surrounding tumour stroma, with the ability to imbibe large amounts of water molecules and create a viscous gel, contributing to high intratumoural pressure and reduced interstitial flow.[57,58] As biological samples are viscoelastic, a decrease in both elastic and viscous components resulted in the decreased complex modulus. Decreased culture elasticity and viscosity demonstrated a possible change in the matrix network topology, which likely resulted in the decreased off-chip PDAC culture viability with increased losartan concentrations. ESI† Fig. S5A shows the PDAC culture viability assessment with the different losartan concentrations.

With different biochemical compositions, signalling molecules and mechanical transduction mechanisms, the ECM modulates several cellular functions, including the cell cycle, cell adhesion, proliferation and migration.[59,60] Changes to the ECM matrix integrity, therefore, affect the homeostasis and functions of cells resulting in the decreased culture viability observed.[59] The reduction in collagen content, reduced mechanical stiffness of the cultures, and a minimum effect on cell viability (69% for the off-chip PDAC culture) confirmed 10 μM losartan to be an optimum concentration to use for on-chip assessments. Investigating this, the effect of gemcitabine only was first assessed against our microfluidic PDAC model, followed by treatment with losartan only to determine how it affected collagen deposition and interstitial flow in our model. Finally, our model was incubated with gemcitabine and losartan together to determine the improved effect of gemcitabine with losartan treatment. ESI† Fig. S6 shows confocal images of the 21-day off-chip PDAC cultures for HIF-1 alpha following treatment with losartan of the different concentrations. Irrespective of concentration, the PDAC cultures were found to express HIF-1 alpha, although the cultures were incubated with losartan for 72 hours, and collagen accumulation in the culture matrix was observed to be reduced for improved transport of nutrients, cytokines and oxygen to the cells. In the presence of oxygen or under normoxic conditions, HIF-1 alpha is reported to degrade rapidly.[61,62] With the expression of HIF-1 alpha observed following losartan treatment of increasing concentration, it was important to investigate the relationship between collagen and interstitial flow towards investigating an increase in gemcitabine effect against the PDAC cancer cells from an improvement in the transport of gemcitabine to the cells.

### The effect of gemcitabine only on the microfluidic PDAC culture model

As shown in Fig. 1, the PDAC cells were seeded into the 5-channel microfluidic device for a mechanically mature 21-day culture prior to treatment with gemcitabine only at a concentration of 31.25 μM. 31.25 μM gemcitabine was found to be an optimum concentration to use based on previous assessments – it resulted in a percentage viability of approximately 70%, providing sufficient cellular viability to assess further viability decreases of gemcitabine and other therapeutics.[13] For comparison, to assess how the dense rigid stroma of the PDAC tumour tissue affects drug efficacy, a 7-day microfluidic PDAC culture was also treated with 31.25 μM gemcitabine. Fig. 7 shows the ATP viability assessment following treatment with gemcitabine. The culture viability of the 21-day microfluidic culture with gemcitabine only treatment (day 21 + gem only treatment) was 62%. For the 7-day microfluidic PDAC culture with gemcitabine only treatment (day 7 + gem only treatment), the culture viability was approximately 9.8%. The percentage decrease in the hydraulic conductivity of the interstitial space of the collagenous 21-day microfluidic PDAC culture compared to the 7-day culture was 82% (Fig. 4). With reduced hydraulic conductivity of the interstitial space of the 21-day culture is reduced drug delivery to cancer cells resulting in decreased gemcitabine efficacy and increased drug resistance. This showed that the collagenous microfluidic PDAC model hampered the effects of gemcitabine as seen off-chip. ESI† Fig. S7 shows the ATP viability assessment of the 21-day PDAC culture, off-chip[13] and on-chip together, following gemcitabine treatment. In addition, further to the physical barrier reduced interstitial flow poses, a rigid hypoxic and acidic environment would inactivate drugs due to the presence of the concentrated glycolytic by-product, lactate.[34,50] As such, it was perceived disrupting the 21-day microfluidic PDAC collagenous microenvironment with losartan, would increase gemcitabine efficacy and reduce drug resistance.

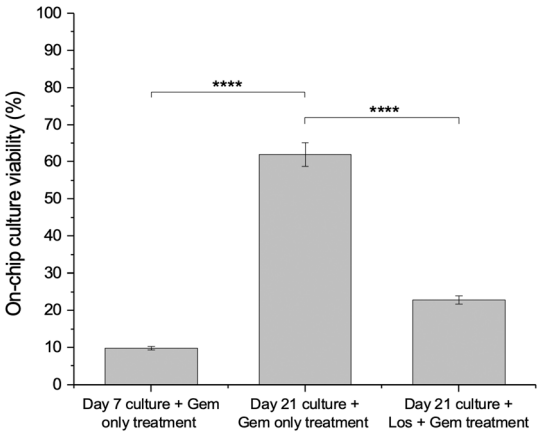


**Fig. 7** The ATP viability assessment of the microfluidic PDAC culture model treated with 31.25 μM gemcitabine only or 31.25 μM gemcitabine and 10 μM losartan together. $N$ = 10 microfluidic PDAC cultures grown for 7 days and treated with gemcitabine only (day 7 + gem only treatment), $n$ = 11 microfluidic PDAC cultures grown for 21 days and treated with gemcitabine only (day 21 + gem only treatment), and $n$ = 6 microfluidic PDAC cultures grown for 21 days and treated with gemcitabine and losartan together (day 21 + Los + gem treatment) all generated from three separate seeding settings. **** $p <$ 0.0001, one-way ANOVA followed by Tukey's multiple comparison test.

**Losartan decreases collagen levels, increases interstitial flow, and improves the efficacy of gemcitabine on the microfluidic PDAC culture model**

Initially, collagen levels and the interstitial flow in the microfluidic PDAC model were investigated with losartan only, at a concentration of 10 μM. Fig. 8A shows images of the collagen type I immunostaining in the microfluidic model with the losartan only treatment – before losartan treatment (no losartan treatment; confocal images as also seen in Fig. 3) and after a 72-hour incubation with losartan (10 μM losartan treatment). Similar to the off-chip PDAC cultures, 10 μM losartan treatment resulted in a more porous collagen network with decreased collagen levels compared to the model with no losartan treatment. Fig. 8B shows the hydraulic conductivity of the interstitial space in the model with losartan only treatment compared with the 21-day model with no losartan treatment and BME gel only. There was improved hydraulic conductivity in the culture interstitial space by approximately 60% for the losartan treated cultures compared to the cultures with no losartan treatment (Table 1). The percentage viability of the model with 10 μM losartan treatment was approximately 91% (ESI† Fig. S5B), showing no adverse effect with losartan treatment.

Increased hydraulic conductivity of the interstitial space permits the interstitial flow of drugs to cells. We hypothesised that with losartan treatment, there will be an increased gemcitabine effect. With reduced collagen, the culture matrix

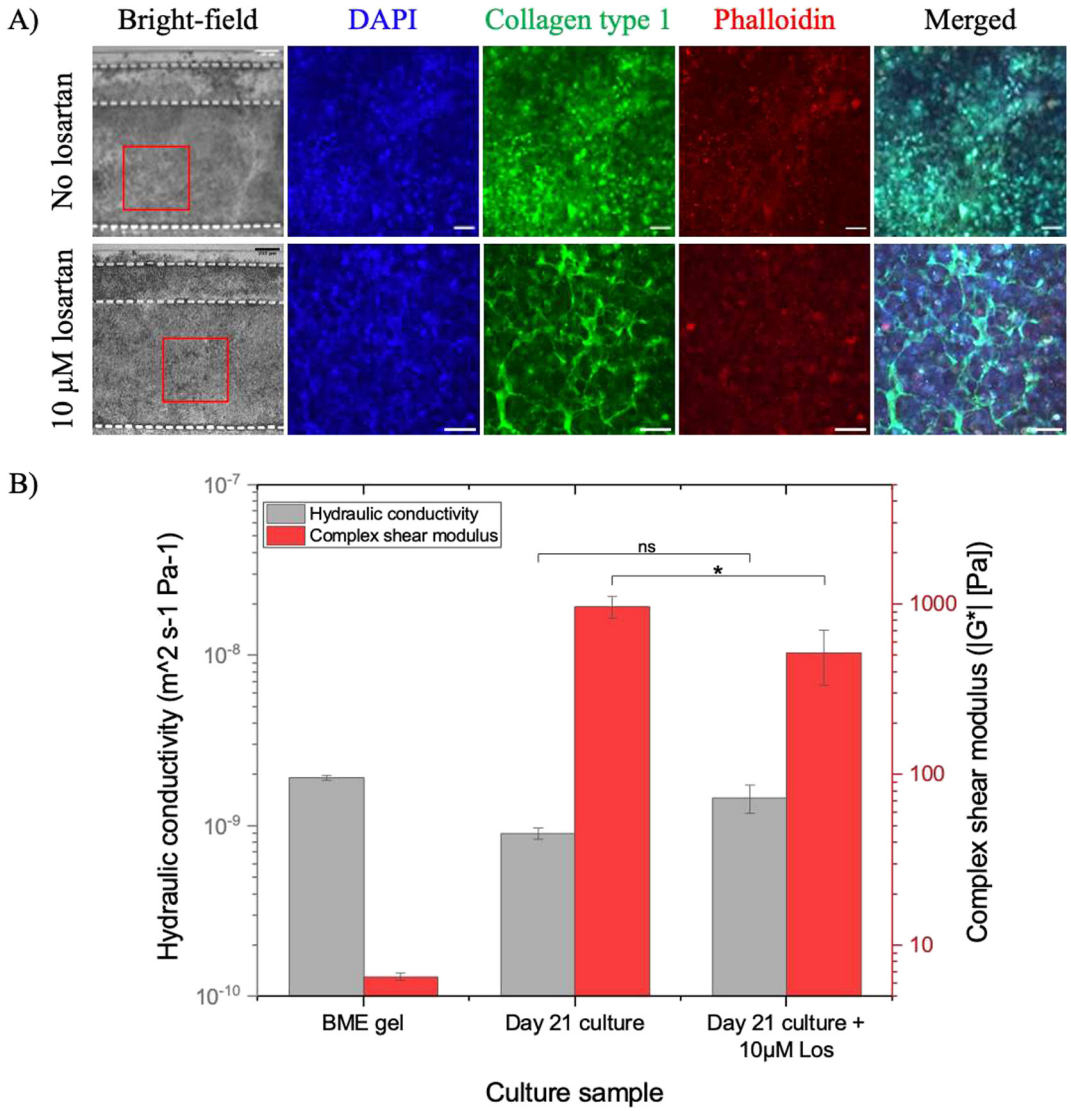


Fig. 8 A) Confocal images of the immunostained 21-day microfluidic PDAC culture model for collagen type 1 in green after 72-hour incubation before (as seen in Fig. 3, day 21) and after a 72-hour incubation with losartan. DAPI in blue and phalloidin in red were used to stain the cell nuclei and the cytoskeleton, respectively. B) The hydraulic conductivity of the interstitial space of the BME gel and 21-day microfluidic PDAC culture model without (data as seen in Fig. 5) and with 10 μM losartan treatment for 72 hours compared to their respective complex shear modulus. $N$ = 3–4 devices with BME gel only or the 21-day microfluidic PDAC culture model from three separate seeding settings. * $p < 0.5$ and *Ns*, $p > 0.5$, one-way ANOVA followed by Tukey's multiple comparison test.

was more porous, resulting in increased interstitial flow and, therefore, drug delivery to the cells. The 21-day microfluidic PDAC cultures were treated with 10 μM losartan for 72 hours and then treated with 31.25 μM gemcitabine for another 72 hours. The percentage viability of the gemcitabine treated model, following losartan treatment, was 23% (Fig. 7, day 21 culture + gem + Los treatment). This demonstrated that matrix-disrupting drugs like losartan improves the delivery and effect of gemcitabine in our microfluidic PDAC model by limiting collagen deposition and increasing interstitial flow.

## Conclusion

The aim of this work was to develop an appropriate microfluidic PDAC model, recapitulating the disease tumour mechanics to investigate gemcitabine efficacy with losartan treatment effectively. Studies have shown PDAC cancer-stroma interactions to influence therapeutic resistance without considering the tumour tissue mechanics critical to drug delivery and their effects. A 5-channel microfluidic device was developed to effectively culture the model and mimic the PDAC rigid, collagenous, and hypoxic microenvironment with reduced interstitial flow. Here, losartan, with its matrix-depleting properties, reduced the levels of collagen in the microfluidic culture model and improved interstitial flow and gemcitabine efficacy. We show how important it is to have culture models with the relevant microphysiological and biophysical hallmarks to test drugs against cancer cells effectively. Only by improving the way we test new therapeutic interventions can we hope to improve patient outcomes in diseases such as pancreatic cancer.

## Data availability

The raw data and supplementary data associated with this article can be found available from **https://doi.org/10.5518/1297**.

## Author contributions

D. K. designed, performed the experiments, and analysed the data, and D. K. and S. A. P. wrote the manuscript with input from all authors.

## Conflicts of interest

There are no conflicts of interest to declare.

## Acknowledgements

The authors would like to acknowledge the Engineering and Physical Sciences Research Council (EP/P023266/1, EP/V026739/1) and the Royal Society of Chemistry (E21-6195497927) for funding this project. We would like to thank Dr Zhang Y. Ong for providing formaldehyde reagent to perform immunostaining and Dr Matt D. G. Hughes for his help and support in understanding the rheological data.

## References

1 A. N. Hosein, R. A. Brekken and A. Maitra, Pancreatic cancer stroma: an update on therapeutic targeting strategies, *Nat. Rev. Gastroenterol. Hepatol.*, 2020, **17**(8), 487–505.
2 D. R. Principe, P. W. Underwood, M. Korc, J. G. Trevino, H. G. Munshi and A. Rana, The Current Treatment Paradigm for Pancreatic Ductal Adenocarcinoma and Barriers to Therapeutic Efficacy, *Front. Oncol.*, 2021, **11**, 688377.
3 T. Y. S. Le Large, M. F. Bijlsma, G. Kazemier, H. W. M. van Laarhoven, E. Giovannetti and C. R. Jimenez, Key biological processes driving metastatic spread of pancreatic cancer as identified by multi-omics studies, *Semin. Cancer Biol.*, 2017, **44**, 153–169.
4 M. Orth, P. Metzger, S. Gerum, J. Mayerle, G. Schneider and C. Belka, *et al.*, Pancreatic ductal adenocarcinoma: biological hallmarks, current status, and future perspectives of combined modality treatment approaches, *Radiat. Oncol.*, 2019, **14**(1), 141.
5 S. P. Pothula, R. C. Pirola, J. S. Wilson and M. V. Apte, Pancreatic stellate cells: Aiding and abetting pancreatic cancer progression, *Pancreatology.*, 2020, **20**(3), 409–418.
6 A. R. Mekapogu, S. P. Pothula, R. C. Pirola, J. S. Wilson and M. V. Apte, Multifunctional role of pancreatic stellate cells in pancreatic cancer, *Ann. Pancreat. Cancer*, 2019, **2**, 10.
7 J. Schnittert, R. Bansal and J. Prakash, Targeting Pancreatic Stellate Cells in Cancer, *Trends Cancer*, 2019, **5**(2), 128–142.
8 B. Piersma, M. K. Hayward and V. M. Weaver, Fibrosis and cancer: A strained relationship, *Biochim. Biophys. Acta, Rev. Cancer*, 2020, **1873**(2), 188356.
9 T. Conroy, P. Hammel, M. Hebbar, M. Ben Abdelghani, A. C. Wei and J. L. Raoul, *et al.*, FOLFIRINOX or Gemcitabine as Adjuvant Therapy for Pancreatic Cancer, *N. Engl. J. Med.*, 2018, **379**(25), 2395–2406.
10 T. D. F. Conroy, M. Ychou, O. Bouché, R. Guimbaud, Y. Bécouarn, A. Adenis, J. L. Raoul, S. Gourgou-Bourgade, C. de la Fouchardière, J. Bennouna, J. B. Bachet, F. Khemissa-Akouz, D. Péré-Vergé, C. Delbaldo, E. Assenat, B. Chauffert, P. Michel, C. Montoto-Grillot and M. Ducreux, PRODIGE Intergroup. FOLFIRINOX *versus* Gemcitabine for Metastatic Pancreatic Cancer, *N. Engl. J. Med.*, 2011, **364**(19), 1817–1825.
11 J. Hoarau-Vechot, A. Rafii, C. Touboul and J. Pasquier, Halfway between 2D and Animal Models: Are 3D Cultures the Ideal Tool to Study Cancer-Microenvironment Interactions?, *Int. J. Mol. Sci.*, 2018, **19**(1), 181.
12 H. F. Tsai, A. Trubelja, A. Q. Shen and G. Bao, Tumour-on-a-chip: microfluidic models of tumour morphology, growth and microenvironment, *J. R. Soc., Interface*, 2017, **14**(131), 20170137.
13 D. Kpeglo, M. D. G. Hughes, L. Dougan, M. Haddrick, M. A. Knowles and S. D. Evans, *et al.*, Modeling the mechanical stiffness of pancreatic ductal adenocarcinoma, *Matrix Biol. Plus*, 2022, 14.
14 B. Diop-Frimpong, V. P. Chauhan, S. Krane, Y. Boucher and R. K. Jain, Losartan inhibits collagen I synthesis and

 

improves the distribution and efficacy of nanotherapeutics in tumors, *Proc. Natl. Acad. Sci. U. S. A.*, 2011, **108**(7), 2909–2914.

15 W.-B. Liu, X.-P. Wang, K. Wu and R.-L. Zhang, Effects of angiotensin II receptor antagonist, Losartan on the apoptosis, proliferation and migration of the human pancreatic stellate cells, *World J. Gastroenterol.*, 2005, **11**(41), 6489–6494.

16 L. Zhang, Y. Wang, T. Xia, Q. Yu, Q. Zhang and Y. Yang, *et al.*, Suppression for lung metastasis by depletion of collagen I and lysyl oxidase *via* losartan assisted with paclitaxel-loaded pH-sensitive liposomes in breast cancer, *Drug Delivery*, 2016, **23**(8), 2970–2979.

17 E. L. Deer, J. Gonzalez-Hernandez, J. D. Coursen, J. E. Shea, J. Ngatia and C. L. Scaife, *et al.*, Phenotype and genotype of pancreatic cancer cell lines, *Pancreas*, 2010, **39**(4), 425–435.

18 M. D. Bourn, D. V. B. Batchelor, N. Ingram, J. R. McLaughlan, P. L. Coletta and S. D. Evans, *et al.*, High-throughput microfluidics for evaluating microbubble enhanced delivery of cancer therapeutics in spheroid cultures, *J. Controlled Release*, 2020, **326**, 13–24.

19 P. A. Janmey, P. C. Georges and S. Hvidt, Basic Rheology for Biologists, *Methods Cell Biol.*, 2007, **83**, 3–27.

20 D. Weitz, H. M. Wyss and R. J. Larsen, Oscillatory Rheology Measuring the Viscoelastic Behaviour of Soft Materials, *GIT Lab. J. Europe*, 2007, **11**, 68–70.

21 C. Wex, M. Frohlich, K. Brandstadter, C. Bruns and A. Stoll, Experimental analysis of the mechanical behavior of the viscoelastic porcine pancreas and preliminary case study on the human pancreas, *J. Mech. Behav. Biomed. Mater.*, 2015, **41**, 199–207.

22 L. J. Liu and M. Schlesinger, Interstitial hydraulic conductivity and interstitial fluid pressure for avascular or poorly vascularized tumors, *J. Theor. Biol.*, 2015, **380**, 1–8.

23 A. Asif, K. H. Kim, F. Jabbar, S. Kim and K. H. Choi, Real-time sensors for live monitoring of disease and drug analysis in microfluidic model of proximal tubule, *Microfluid. Nanofluid.*, 2020, **24**(6), 43.

24 D. Microfluidics, Shear stress in microfluidic devices–Darwin Microfluidics, 2017.

25 A. J. Rice, E. Cortes, D. Lachowski, B. C. H. Cheung, S. A. Karim and J. P. Morton, *et al.*, Matrix stiffness induces epithelial-mesenchymal transition and promotes chemoresistance in pancreatic cancer cells, *Oncogenesis*, 2017, **6**(7), e352.

26 G. Follain, D. Herrmann, S. Harlepp, V. Hyenne, N. Osmani and S. C. Warren, *et al.*, Fluids and their mechanics in tumour transit: shaping metastasis, *Nat. Rev. Cancer*, 2020, **20**(2), 107–124.

27 M. Beer, N. Kuppalu, M. Stefanini, H. Becker, I. Schulz and S. Manoli, *et al.*, A novel microfluidic 3D platform for culturing pancreatic ductal adenocarcinoma cells: comparison with *in vitro* cultures and *in vivo* xenografts, *Sci. Rep.*, 2017, **7**(1), 1325.

28 M. J. Bradney, S. M. Venis, Y. Yang, S. F. Konieczny and B. Han, A Biomimetic Tumor Model of Heterogeneous Invasion in Pancreatic Ductal Adenocarcinoma, *Small*, 2020, **16**(10), e1905500.

29 C. R. Drifka, K. W. Eliceiri, S. M. Weber and W. J. Kao, A bioengineered heterotypic stroma-cancer microenvironment model to study pancreatic ductal adenocarcinoma, *Lab Chip*, 2013, **13**(19), 3965–3975.

30 J. H. Lee, S. K. Kim, I. A. Khawar, S. Y. Jeong, S. Chung and H. J. Kuh, Microfluidic co-culture of pancreatic tumor spheroids with stellate cells as a novel 3D model for investigation of stroma-mediated cell motility and drug resistance, *J. Exp. Clin. Cancer Res.*, 2018, **37**(1), 4.

31 C. C. Lin and M. Korc, Designer hydrogels: Shedding light on the physical chemistry of the pancreatic cancer microenvironment, *Cancer Lett.*, 2018, **436**, 22–27.

32 J. S. Lowe and P. G. Anderson, Support Cells and the Extracellular Matrix, *Stevens Lowes Human Histology*, 2015, pp. 55–70.

33 L. T. Baxter and R. K. Jain, Transport of fluid and macromolecules in tumors. I. Role of interstitial pressure and convection, *Microvasc. Res.*, 1989, **37**(1), 77–104.

34 R. K. Jain, J. D. Martin and T. Stylianopoulos, The role of mechanical forces in tumor growth and therapy, *Annu. Rev. Biomed. Eng.*, 2014, **16**, 321–346.

35 J. M. Munson and A. C. Shieh, Interstitial fluid flow in cancer: implications for disease progression and treatment, *Cancer Manage. Res.*, 2014, **6**, 317–328.

36 S. Majumder, M. T. Islam and R. Righetti, Non-invasive imaging of interstitial fluid transport parameters in solid tumors *in vivo*, *Sci. Rep.*, 2023, **13**(1), 7132.

37 F. L. Lai Benjamin, X. Lu Rick, Y. Hu, H. L. Davenport, W. Dou and E. Y. Wang, *et al.*, Recapitulating pancreatic tumor microenvironment through synergistic use of patient organoids and organ-on-a-chip vasculature, *Adv. Funct. Mater.*, 2020, **30**(48), 2000545.

38 B. Kramer, L. Haan, M. Vermeer, T. Olivier, T. Hankemeier and P. Vulto, *et al.*, Interstitial Flow Recapitulates Gemcitabine Chemoresistance in A 3D Microfluidic Pancreatic Ductal Adenocarcinoma Model by Induction of Multidrug Resistance Proteins, *Int. J. Mol. Sci.*, 2019, **20**(18), 4647.

39 Q. Ji, Y. L. Wang, L. M. Xia, Y. Yang, C. S. Wang and Y. Q. Mei, High shear stress suppresses proliferation and migration but promotes apoptosis of endothelial cells co-cultured with vascular smooth muscle cells *via* down-regulating MAPK pathway, *J. Cardiothorac. Surg.*, 2019, **14**(1), 216.

40 P. Juhl, S. Bondesen, C. L. Hawkins, M. A. Karsdal, A. C. Bay-Jensen and M. J. Davies, *et al.*, Dermal fibroblasts have different extracellular matrix profiles induced by TGF-beta, PDGF and IL-6 in a model for skin fibrosis, *Sci. Rep.*, 2020, **10**(1), 17300.

41 M. V. Plikus, X. Wang, S. Sinha, E. Forte, S. M. Thompson and E. L. Herzog, *et al.*, Fibroblasts: Origins, definitions, and functions in health and disease, *Cell*, 2021, **184**(15), 3852–3872.

42 P. Phillips, Pancreatic stellate cells and fibrosis. BTI-Pancreatic Cancer and Tumor Microenvironment, 2012.

43 P. H. Maxwell, The HIF pathway in cancer, *Semin. Cell Dev. Biol.*, 2005, **16**(4–5), 523–530.
44 V. Petrova, M. Annicchiarico-Petruzzelli, G. Melino and I. Amelio, The hypoxic tumour microenvironment, *Oncogenesis*, 2018, **7**(1), 10.
45 X. Zhao, S. Gao, H. Ren, W. Sun, H. Zhang and J. Sun, *et al.*, Hypoxia-inducible factor-1 promotes pancreatic ductal adenocarcinoma invasion and metastasis by activating transcription of the actin-bundling protein fascin, *Cancer Res.*, 2014, **74**(9), 2455–2464.
46 S. J. Kierans and C. T. Taylor, Regulation of glycolysis by the hypoxia-inducible factor (HIF): implications for cellular physiology, *J. Physiol.*, 2021, **599**(1), 23–37.
47 G. N. Masoud and W. Li, HIF-1alpha pathway: role, regulation and intervention for cancer therapy, *Acta Pharm. Sin. B*, 2015, **5**(5), 378–389.
48 P. H. Maxwell, C. W. Pugh and P. J. Ratcliffe, Activation of the HIF pathway in cancer, *Curr. Opin. Genet. Dev.*, 2001, **11**(3), 293–299.
49 A. Laitala and J. T. Erler, Hypoxic Signalling in Tumour Stroma, *Front. Oncol.*, 2018, **8**, 189.
50 E. Kaemmerer, D. Loessner and V. M. Avery, Addressing the tumour microenvironment in early drug discovery: a strategy to overcome drug resistance and identify novel targets for cancer therapy, *Drug Discovery Today*, 2021, **26**(3), 663–676.
51 M. C. Lampi and C. A. Reinhart-King, Targeting extracellular matrix stiffness to attenuate disease: From molecular mechanisms to clinical trials, *Sci. Transl. Med.*, 2018, **10**(422), eaao 0475.
52 V. P. Chauhan, J. D. Martin, H. Liu, D. A. Lacorre, S. R. Jain and S. V. Kozin, *et al.*, Angiotensin inhibition enhances drug delivery and potentiates chemotherapy by decompressing tumour blood vessels, *Nat. Commun.*, 2013, **4**, 2516.
53 F. Burla, Y. Mulla, B. E. Vos, A. Aufderhorst-Roberts and G. H. Koenderink, From mechanical resilience to active material properties in biopolymer networks, *Nat. Rev. Phys.*, 2019, **1**(4), 249–263.
54 T. R. Cox, The matrix in cancer, *Nat. Rev. Cancer*, 2021, **21**(4), 217–238.
55 M. W. Pickup, J. K. Mouw and V. M. Weaver, The extracellular matrix modulates the hallmarks of cancer, *EMBO Rep.*, 2014, **15**(12), 1243–1253.
56 D. Kudo, A. Suto and K. Hakamada, The Development of a Novel Therapeutic Strategy to Target Hyaluronan in the Extracellular Matrix of Pancreatic Ductal Adenocarcinoma, *Int. J. Mol. Sci.*, 2017, **18**(3), 600.
57 P. P. Provenzano and S. R. Hingorani, Hyaluronan, fluid pressure, and stromal resistance in pancreas cancer, *Br. J. Cancer*, 2013, **108**(1), 1–8.
58 K. Tahkola, M. Ahtiainen, J. P. Mecklin, I. Kellokumpu, J. Laukkarinen and M. Tammi, *et al.*, Stromal hyaluronan accumulation is associated with low immune response and poor prognosis in pancreatic cancer, *Sci. Rep.*, 2021, **11**(1), 12216.
59 J. Nicolas, S. Magli, L. Rabbachin, S. Sampaolesi, F. Nicotra and L. Russo, 3D Extracellular Matrix Mimics: Fundamental Concepts and Role of Materials Chemistry to Influence Stem Cell Fate, *Biomacromolecules*, 2020, **21**(6), 1968–1994.
60 K. M. Yamada, A. D. Doyle and J. Lu, Cell-3D matrix interactions: recent advances and opportunities, *Trends Cell Biol.*, 2022, **32**(10), 883–895.
61 D. M. Stroka, T. Burkhardt, I. Desbaillets, R. H. Wenger, D. A. H. Neil and C. Bauer, *et al.*, HIF-1 is expressed in normoxic tissue and displays an organ-specific regulation under systemic hypoxia, *FASEB J.*, 2001, **15**(13), 2445–2453.
62 A. Weidemann and R. S. Johnson, Biology of HIF-1alpha, *Cell Death Differ.*, 2008, **15**(4), 621–627.